Atmos. Chem. Phys. Discuss., 15, 3667–3702, 2015
www.atmos-chem-phys-discuss.net/15/3667/2015/
doi:10.5194/acpd-15-3667-2015

Atmospheric Chemistry and Physics Discussions

Experimental investigation of ion-ion recombination at atmospheric conditions

A. Franchin[1], S. Ehrhart[2], J. Leppä[3,4], T. Nieminen[1,5], S. Gagné[6,7], S. Schobesberger[1], D. Wimmer[1], J. Duplissy[5], F. Riccobono[8], E. Dunne[9], L. Rondo[10], A. Downard[4], F. Bianchi[8,11], A. Kupc[12], G. Tsagkogeorgas[13], K. Lehtipalo[1], H. E. Manninen[1], J. Almeida[2], A. Amorim[14], P. E. Wagner[12], A. Hansel[15,16], J. Kirkby[2,10], A. Kürten[10], N. M. Donahue[17], V. Makhmutov[18], S. Mathot[2], A. Metzger[15], T. Petäjä[1], R. Schnitzhofer[16], M. Sipilä[1], Y. Stozhkov[18], A. Tomé[14], V.-M. Kerminen[1,3], K. Carslaw[19], J. Curtius[10], U. Baltensperger[8], and M. Kulmala[1]

[1]Department of Physics, P.O. Box 64, 00014 University of Helsinki, Finland
[2]CERN, 1211 Geneva, Switzerland
[3]Finnish Meteorological Institute, Atmospheric Composition Research, P.O. Box 503, 00101 Helsinki, Finland
[4]California Institute of Technology, Department of Chemical Engineering, 1200 E. California Blvd., Mail Code 101-20, Pasadena, 91125, US
[5]Helsinki Institute of Physics, Helsinki, Finland
[6]Department of Physics and Atmospheric Science, Dalhousie University, Halifax, B3H 3J5, Canada

[7]Environment Canada, Downsview, Toronto, M3H 5T4, Canada
[8]Paul Scherrer Institute, 5232 Villigen, Switzerland
[9]Finnish Meteorological Institute, Kuopio Unit, P.O.Box 1627, 70211 Kuopio, Finland
[10]Institute for Atmospheric and Environmental Sciences, Goethe University Frankfurt, Altenhöferallee 1, 60438 Frankfurt am Main, Germany
[11]Institute for Atmospheric and Climate Science, ETH Zurich, 8092 Zurich, Switzerland
[12]University of Vienna, Universitätsring 1, 1010 Wien, Austria
[13]Leibniz Institute for Tropospheric Research, Permoserstr. 15, 04318 Leipzig, Germany
[14]CENTRA-SIM, F.C.U. Lisboa and U. Beira Interior, Portugal
[15]Ionicon Analytik GmbH, 6020 Innsbruck, Austria
[16]University of Innsbruck, Institute for Ion and Applied Physics, 6020 Innsbruck, Austria
[17]Center for Atmospheric Particle Studies, Carnegie Mellon University, Pittsburgh, PA 15213, USA
[18]Solar and Cosmic Ray Research Laboratory, Lebedev Physical Institute, Moscow, Russia
[19]School of Earth and Environment, University of Leeds, LS2 9JT Leeds, UK

Received: 1 December 2014 – Accepted: 16 January 2015 – Published: 9 February 2015

Correspondence to: A. Franchin (alessandro.franchin@helsinki.fi)

Published by Copernicus Publications on behalf of the European Geosciences Union.

Abstract

We present the results of laboratory measurements of the ion-ion recombination coefficient at different temperatures, relative humidities and concentrations of ozone and sulfur dioxide. The experiments were carried out using the Cosmics Leaving OUtdoor Droplets (CLOUD) chamber at CERN, the walls of which are made of conductive material, making it possible to measure small ions. We produced ions in the chamber using a 3.5 GeV c^{-1} beam of positively-charged pions (π^+) from the CERN Proton Synchrotron (PS) and with galactic cosmic rays, when the PS was switched off. The range of the ion production rate varied from 2 to 100 cm^{-3} s^{-1}, covering the typical range of ionization throughout the troposphere. The temperature ranged from −55 to 20 °C, the relative humidity from 0 to 70 %, the SO_2 concentration from 0 to 40 ppb, and the ozone concentration from 200 to 700 ppb. At 20 °C and 40 % RH, the retrieved ion-ion recombination coefficient was $(2.3 \pm 0.7) \times 10^{-6}$ cm^3 s^{-1}. We observed no dependency of the ion-ion recombination coefficient on ozone concentration and a weak variation with sulfur dioxide concentration. However, we found a strong dependency of the ion-ion recombination coefficient on temperature. We compared our results with three different models and found an overall agreement for temperatures above 0 °C, but a disagreement at lower temperatures. We observed a strong dependency of the recombination coefficient on relative humidity, which has not been reported previously.

1 Introduction

Air ions are fundamental to atmospheric electricity and play a central role in the proposed connection between solar activity, Galactic Cosmic Rays (GCRs) and climate (Israël, 1970; Carslaw et al., 2002; Usoskin and Kovaltsov, 2009). Ions are known to enhance nucleation rates in atmospherically relevant vapor mixtures (Kirkby et al., 2011), but the overall effect of ions on atmospheric new particle formation (NPF) and subsequent cloud condensation nuclei production has remained a controversial issue (Gagné

ACPD
15, 3667–3702, 2015

et al., 2008; Kazil et al., 2010; Manninen et al., 2010; Yu et al., 2010; Hirsikko et al., 2011; Kontkanen et al., 2013; Kulmala et al., 2013). Air ions accumulating near cloud edges may affect cloud microphysics and ultimately climate via several mechanisms that are currently poorly quantified (Tinsley, 2000; Harrison and Ambaum, 2008).

Atmospheric ions are usually classified in three groups depending on their diameter (here, all diameters are reported as Millikan–Fuchs equivalent mobility diameters, Mäkelä et al., 1996): small ions (< 1.9 nm), intermediate ions (1.9–7.7 nm) and large ions (> 7.7 nm). In terms of mobility, they are classified as: small ions ($> 0.57\,cm^2\,V^{-1}\,s^{-1}$), intermediate ions ($4.3\times10^{-2}$–$0.57\,cm^2\,V^{-1}\,s^{-1}$) and large ions ($< 4.3\times10^{-2}\,cm^2\,V^{-1}$) (Hõrrak et al., 2000). Small ions have a high mobility, thus they take the most active part in the transfer of charge throughout the atmosphere (Chalmers, 1949; Ogawa, 1985) and play a role in NPF and in aerosol charging processes (Adachi and Kousaka, 1985; Manninen et al., 2011). This work focuses on small ions, from here on simply referred to as "ions" unless specified otherwise.

Air ions are continuously produced in the atmosphere from GCRs and terrestrial sources, such as radon decay and gamma radiation from the soil (Laakso et al., 2004). Within the planetary boundary layer, terrestrial sources play an important role in ionization processes, whereas in the whole troposphere GCRs are the dominant source of ions (Harrison and Carslaw, 2003; Kazil and Lovejoy, 2004; Arnold, 2008; Zhang et al., 2011; Williams et al., 2011). When ionizing radiation interacts with the air, a primary positive ion (e.g., N_2^+, O_2^+) and an electron are generated (Smith and Spanel, 1995). The positive ion has roughly the same diffusion coefficient as the surrounding molecules. After the interaction with the ionizing radiation, its change in momentum is negligible and we can picture it as in Brownian motion around its initial position. The electron, however, gains a finite momentum in the interaction. It starts to interact with atmospheric molecules, exciting and ionizing them, until its energy decreases and it binds to an electro-negative molecule, for example O_2, creating O_2^-. This process takes place in a few nanoseconds. Once two molecular ions of opposite polarity are created, they can interact with molecules that have higher electronegativity or proton

ACPD
15, 3667–3702, 2015

affinity (e.g., H_2O) and transfer their charge, or they can establish hydrogen or other chemical bonds with other molecules and cluster (Smith and Spanel, 1995). It is only at this point that ions are considered stable and measurable.

The number concentration of ions depends on the balance between ion sources and sinks, i.e., on the production and loss rate at a given time and condition. The production rate is proportional to the amount of ionizing radiation present, whereas the loss mechanisms depend on the ion-aerosol attachment rate, on the rate of attachment to macroscopic surfaces and on the ion-ion recombination rate (Tammet et al., 2006). The ion-ion recombination rate is the rate at which two ions of opposite charge collide with each other and get neutralized. It depends on the mobility of ions and possibly on their chemical composition and ambient conditions. Ion-ion recombination becomes dominant in extremely clean environments, where the integral of the aerosol surface distribution is negligible with respect to the ion-ion recombination rate, and the probability for ion-aerosol attachment is low (Volland, 1995). Recombination is also important at high ionization rates, when the production of ion pairs is so high that the probability of colliding with a neutral aerosol particle is minimal with respect to the probability of colliding with an ion of opposite charge.

The aim of this work is to determine the ion-ion recombination coefficient under different conditions. In past studies, the ion-ion recombination rate was calculated for understanding aerosol diffusion charging (Natanson, 1960; Bates and Flannery, 1969) and it was measured primarily for dosimetry purposes (McGowan, 1965, and references therein). In most cases, the ions were studied in noble gases or in pure oxygen. The present work is the first laboratory experiment performed at conditions close to those found in the Earth's atmosphere that presents quantitative results about the ion-ion recombination coefficient at varying temperature, relative humidity and trace gas concentrations.

ACPD
15, 3667–3702, 2015

2 Experimental methods

The typical experiment carried out consisted of measuring the ion concentrations at several beam intensities, each time for long enough (about 30 min) to reach steady state conditions while all the other variables were kept constant. The beam intensity was varied from 0 to 1.5×10^5 pions s^{-1}, corresponding to an IPR ranging from about 2 to 100 ion pairs $cm^{-3}\,s^{-1}$. The concentration of aerosol particles was below 30 cm^{-3} and the concentration of ions with $D_p > 1.9$ nm was negligible as the experiments were carried out in an aerosol-free chamber. Usually, the beam settings were increased consecutively, generating a series of steps of IPR. Each time, at the end of the last step, the beam shutter was closed, and we observed the ion concentration decay (Fig. 2). The size range of the ions considered in this study was 3.2–0.57 $cm^2\,V^{-1}\,s^{-1}$, i.e., 0.8–1.9 nm in mobility equivalent diameter (D_p). In this analysis the signal of the NAIS in ion mode was integrated over all the channels corresponding to $D_p < 1.9$ nm. The rest of the ion number size distribution was not considered, as it was zero. From this dataset, we retrieved the ion-ion recombination coefficient under different conditions.

2.1 The CLOUD chamber

The Cosmics Leaving OUtdoor Droplets (CLOUD) chamber (Kirkby et al., 2011) is a cylindrical vessel with a diameter of 3 m and a volume of 26.1 m^3 made of electro-polished 316L stainless steel (Fig. 1c). Its walls are conductive, which makes it possible to measure small ions that, in a traditional aerosol chamber made of polytetrafluoroethylene (PTFE), would be removed in less than one second by the parasitic electric fields created by the dielectric material (McMurry and Rader, 1985). In the interior of the chamber, all plastic components are avoided using copper o-rings and metallic coating on electrically insulating components. When it is necessary to work in an ion-free environment, two circular grids, one located at the top and one at the bottom of the chamber, are provided with a potential difference of up to 60 kV, generating an ax-

ACPD
15, 3667–3702, 2015

ial electric field able to remove the small ions in less than 0.2 s. When the two circular grids are not in use, they are grounded to avoid ground loops or parasitic electric fields.

The total in-flow to the chamber varies between 100 and 150 L min^{-1}. Most of the flow is taken by the instruments connected to the chamber and a portion of it is purged through a valve that controls the pressure inside the chamber. The chamber is kept at 5 mbar above the atmospheric pressure to avoid contamination from the outside. The chamber is equipped with an ultraviolet fiber-optic system that is installed at the top plate of the chamber, allowing OH production (Kupc et al., 2011) without heating up the chamber. The temperature is controlled by air circulating between the chamber and the insulation surrounding it. The temperature ranges from −80 to 100 °C with a stability inside the chamber of ±0.1 °C for each experiment. The chamber is filled with ultra-pure synthetic air, consisting of N_2 and O_2, obtained from the evaporation of liquid samples. The air is humidified with a Nafion system, using water purified by recirculation through Millipore Super-Q filters and irradiated with UV radiation. Ozone is produced by illuminating a portion of the incoming dry air with UV light. The other trace gases, such as SO_2 and NH_3, are added from gas cylinder reservoirs. These measures aim for the cleanest possible laboratory conditions (Schnitzhofer et al., 2014).

2.2 The particle beam

The particle beam is produced at the CERN Proton Synchrotron. The CLOUD chamber can be exposed to a 3.5 GeV c^{-1} positively-charged pion (π^+) beam produced by a secondary target of aluminium or copper (Duplissy et al., 2010). The intensity of the particle beam can be varied to cover the full range of ionization in the troposphere, from an Ion Production Rate (IPR) of about 2 cm^{-3} s^{-1}, equivalent to boundary layer levels, to 80 cm^{-3} s^{-1}, equivalent to the levels in the free troposphere (Kazil and Lovejoy, 2004; Zhang et al., 2011). The beam consists of pions and muons that have approximately the same energy of about 3.5 GeV and come in spills. Each spill lasts for a few microseconds and delivers 10^8 pions at a time, at intervals of 20 s.

ACPD
15, 3667–3702, 2015

We varied the beam intensity, and thus the IPR in the chamber, by varying the aperture of the beam collimator, which consists of two mechanical jaws made of concrete that can slide vertically and horizontally. At full aperture (60 mm × 60 mm) we have the maximum flux of pions through the chamber. When the collimator was partially closed we reduced the flux of pions and we illuminated a smaller part of the chamber. When the collimator was closed, almost no pion could reach the chamber. In this case, only GCRs, which are passing through the chamber vertically, and some residual pions that pass the blocker, hitting the chamber horizontally, were responsible for the ionization. For this reason, the IPR in the chamber at GCR conditions was about 30 % higher than it would be if the accelerator had been shut down completely.

The pion beam is deliberately defocused to maximize the area where the ionization takes place (Fig. 1c, shaded area). About 70 % of the volume of the chamber is directly ionized and the two mixing fans produce a uniform distribution of ions inside the chamber. The mixing time inside the chamber is estimated to be between 1.7 and 3.6 min (Voigtländer et al., 2012).

2.3 The hodoscope and the B1.2 counter

The hodoscope is an array of scintillation detectors. It measures the pion flux through the chamber and gives accurate positional information on the particle beam. It consists of 9 plastic scintillator slabs adjacent to one another in a vertical orientation and 9 plastic scintillator slabs oriented horizontally (Mizin et al., 2011). The vertical and horizontal slabs form a grid orthogonal to the particle beam, covering an area of about 2 m × 2 m. An ionizing particle, hitting a point on this grid, is located by measuring the coincidence of the signal of two detectors (one vertical and one horizontal). The B1.2 counter consists of two scintillation detectors placed right in front of the beam aperture. It also measures the coincidence of the signal of two detectors in order to count only the pions from the beam. From the number of particles measured per unit time and from the location of the crossed scintillators, we can independently retrieve the beam intensity (Hz) and its horizontal and vertical profile. This allows us to discriminate be-

ACPD
15, 3667–3702, 2015

tween high energy particles coming from the beam, which travel almost horizontally, and the GCRs.

2.4 Neutral cluster and Air Ion Spectrometer (NAIS)

The Neutral cluster and Air Ion Spectrometer (NAIS, Kulmala et al., 2007; Mirme and Mirme, 2013) is manufactured by Airel Ltd in Estonia and measures atmospheric ions in the range [0.8–42] nm and total aerosol particle population in the range [2.5–42] nm. It consists of two cylindrical Differential Mobility Analysers (DMAs) working in parallel, classifying negative and positive ions at the same time (Manninen et al., 2009). The ions are simultaneously classified according to their mobility and detected by a stack of 21 electrometer rings for each analyser. The device is equipped with a unipolar charging unit for each analyser that can be switched on and off.

During the CLOUD experiments, the instrument operated in three modes: particle, ion and offset. In particle mode the main charging unit is turned on. In ion mode the main charging unit is turned off. In offset mode the main charger unit stays off and a filter unit is turned on to make a zero measurement. This zero measurement is used to determine the net signal due to ions and particles. To maximize the flow in the tube and reduce the diffusion losses, the NAIS and a mass spectrometer shared part of the 2.54 cm outer diameter sampling line. Outside the chamber, the flow was split (20 L min^{-1} to the NAIS, 10 L min^{-1} to the APi-TOF) using a Y union (Fig. 1b).

The NAIS operates at a 54 L min^{-1} total inlet flow. The high intake of the NAIS is a challenge in aerosol chamber experiments, where it is required to minimize the amount of air withdrawn. For this reason, the NAIS was operated with a recirculation system, which diluted the inlet flow with filtered air coming from the exhaust of the instrument. The filtered air formed an annulus around the sample flow (Fig. 1a). The use of the dilution system allowed us to reduce the withdrawn flow from the chamber from 54 to 20–30 L min^{-1}. In this study, we only present the data recorded in ion mode, in particular the data from of the first 9 electrometers that collect ions with mobility diame-

ACPD
15, 3667–3702, 2015

ter smaller than 1.9 nm (small ions). The detailed setup used for this work is presented in Fig. 1.

3 Theoretical methods

3.1 Calculation of the ion-ion recombination rate

Using the balance equation at steady state, the ion-ion recombination rate and a linear loss term were determined using the measured ion concentration and the IPR. We can describe the ionization processes inside the chamber using the following balance equation:

$$\frac{dn_{\pm}}{dt} = q - \alpha n_{+} n_{-} - \beta_{\pm} n_{\pm} - k_{CS}(N, D_p) n_{\pm}, \quad (1)$$

where $n_{\pm}$ is the absolute concentration of positive or negative small ions (cm^{-3}), q is the ion production rate (IPR, $cm^{-3}\,s^{-1}$), α is the recombination coefficient ($cm^{3}\,s^{-1}$), β is a first order loss term (s^{-1}) that describes the ion-wall interactions in the aerosol chamber, and other loss mechanisms of the first order, k_{CS} is the coagulation sink, i.e., the rate at which ions are lost by diffusion onto aerosol particles (s^{-1})(Kulmala et al., 2001; Leppä et al., 2011). At a constant IPR, the steady state that is eventually reached depends on the values of α, β and k_{CS}.

We can make some assumptions to simplify Eq. (1). By assuming that $n_{-} \simeq n_{+}$, and that the ion loss by coagulation is negligible compared with the other sink terms, we get:

$$\frac{dn}{dt} = q - \alpha n^2 - \beta n, \quad (2)$$

These assumptions were well posed in our case, since the difference between the number concentration of positive and negative ions was only about 10 % (see Fig. 2)

ACPD
15, 3667–3702, 2015

and during our experiments k_{CS} was constantly below $3 \times 10^{-7}\,s^{-1}$, due to negligible aerosol concentration in the chamber. The solution of Eq. (2) can be found analytically (see Appendix A):

$$n(t) = \frac{n_1(n_0 - n_2) - n_2(n_0 - n_1)\exp\left(-t\sqrt{\beta^2 + 4\alpha q}\right)}{(n_0 - n_2) - (n_0 - n_1)\exp\left(-t\sqrt{\beta^2 + 4\alpha q}\right)}, \quad (3)$$

where n_0 is the concentration of ions at $t = 0$, $n_1 = \frac{-\beta + \sqrt{\beta^2 + 4\alpha Q}}{2\alpha}$ and $n_2 = \frac{-\beta - \sqrt{\beta^2 + 4\alpha Q}}{2\alpha}$.

If we consider steady state conditions, $\frac{dn}{dt} = 0$, Eq. (2) becomes a second order polynomial. The recombination coefficient α, and the linear loss term loss term β, can be retrieved by fitting a second order polynomial function to the data, treating them as free parameters. The ion concentration was set to zero at IPR equal to zero. The linear loss term was retrieved for each given condition and, when the statistic was too poor to determine the linear loss term, we assumed β to be equal to $(8.3 \pm 1.6) \times 10^{-3}\,s^{-1}$, the value retrieved from the dataset with the best statistics (Fig. 5).

Equation (3) was used to check the values of α and β retrieved at steady state by comparing the resulting $n(t)$ to the ion decay data (Fig. 3). The IPR from the beam (q_b) was calculated using the following equation (Duplissy et al., 2010):

$$q_b = N_b I L / V, \quad (4)$$

where N_b is the number of pions per unit time that go through the chamber that can vary between 0 and $1.5 \times 10^6\ s^{-1}$, $I = 61$ i.p. cm^{-1} is the mean ionization per cm for a 3.5 GeV c^{-1} π^+ in air at s.t.p. (Smirnov, 2005), $L = 284$ cm is the path length of a beam particle in the chamber, and $V = 26.1 \times 10^6\,cm^3$ is the chamber volume. The IPR was scaled for different air density at different temperatures.

We used a value of $1.84\,cm^{-3}\,s^{-1}$ for the intensity of the GCRs. The total ion production rate q is given by the sum of the GCR contribution q_0 and the beam contribution

ACPD
15, 3667–3702, 2015

q_b, $q = q_0 + q_b$. The ion concentration was corrected for sample dilution, due to the dilution system described in Sect. 2.4.

3.2 Modelled ion-ion recombination coefficient

The temperature dependency of the calculated ion-ion recombination coefficient was compared to the values computed using three different model approaches. The first model derived by J. J. Thomson (Gardner, 1938; Loeb, 1955; Thomson and Thomson, 2013) considers recombination governed mainly by Brownian motion of ions and molecules and computes the recombination coefficient as:

$$\alpha = \sqrt{2}\pi d^2 C \epsilon. \tag{5}$$

Where $C = \sqrt{3k_bT/m}$ is the root mean square thermal velocity of the ions, $d = e^2/[(3/2)k_BT]$ is the distance where the Coulomb potential energy between the two ions of opposite polarity is equal to their thermal kinetic energy, and ϵ is the probability of the two ions to recombine once they are at distance d. As derived by Thomson, $\epsilon = 2w - w^2$, $w = 1 - 2[1 - \exp(-x)(x+1)]/x^2$, $x = 2d/L$ and L is the mean free path of the ions. The equation for α then becomes:

$$\alpha(\mathrm{cm^3\,s^{-1}}) = 1.90 \times 10^{-5}(273/T)^{\frac{3}{2}} 3/2\sqrt{1/M}\epsilon, \tag{6}$$

when T is the temperature in Kelvin and M is the mass of the ion in Da.

The second model taken into consideration and compared with our experimental data is described by López-Yglesias and Flanagan (2013). Based on Hoppel and Frick (1986), this model was developed for ion-aerosol attachment, but it can be used to compute the recombination coefficient, if we use an aerosol that is as small as the ion and with opposite charge. The model accounts for Brownian motion, Coulombic interaction, image charging, polarization of the molecules and three-body trapping.

ACPD
15, 3667–3702, 2015

The third model, by Brasseur and Chatel (1969), is a parametrization used for describing the ions in the stratosphere based on earlier work by Bates (1982) and Smith and Adams (1982) that has the expression

$$\alpha(\mathrm{cm^3\,s^{-1}}) = 6\times10^{-8}\sqrt{300/T} + 6\times10^{-26}[M_{\mathrm{air}}](300/T)^4, \quad (7)$$

where $[M_{\mathrm{air}}]$ is the concentration of air molecules in $\mathrm{cm^{-3}}$.

4 Results and discussion

The ion-ion recombination was measured in the CLOUD chamber at different temperatures, relative humidities and concentrations of ozone and sulfur dioxide. We obtain a value of $2.3\pm0.7\times10^{-6}\,\mathrm{cm^3\,s^{-1}}$, at 298 K and RH = 40 %, higher than the constant value of $1.6\times10^{-6}\,\mathrm{cm^3\,s^{-1}}$ usually reported in the literature (Laakso et al., 2004). Interestingly, we found that α depends on both temperature and relative humidity (Tables 2 and 1). Figure 4 shows the results of four sets of experiments, where the ion concentration was measured as a function of IPR. For each set of experiments, we kept all the parameters constant except the one under investigation: the concentration of ozone (200–700 ppb), sulfur dioxide (0–50 ppb), temperature (218, 248, 278 and 293 K) and relative humidity (0, 7, 40 and 70 %). The measured recombination rate showed a strong dependency (about a factor of 5 change) on temperature and relative humidity and, to some extent (a factor of 2), on the concentration of sulfur dioxide. The variability in the ozone concentration appeared to have little influence, if any, on the measured recombination rate.

The retrieved loss rate for ions ($8.3\times10^{-3}\,\mathrm{s^{-1}}$, Fig. 5), differs markedly from the linear loss rate retrieved for the sulfuric acid neutral monomer ($1.7\times10^{-3}\,\mathrm{s^{-1}}$, Almeida et al., 2013). This difference between the loss rates might be partially explained by the image charge effect of the ions with the chamber walls, even though this remains a controversial topic (McMurry and Rader, 1985; Mayya and Sapra, 2002; Vauge, 2002;

ACPD
15, 3667–3702, 2015

Chang et al., 2012). Losses might be due to some non-ideal behavior, e.g., retention of surface charge, of some insulator in the clearing field cage region or in proximity to the mixing fans. Yet another possibility is that the mixing in the chamber influences the ion concentrations, creating a higher linear loss rate. Finally, it is possible that sulfuric acid is not lost to the walls with unit efficiency.

4.1 Temperature and relative humidity dependency of the recombination rate

The strongest effect we observed was an increase in the ion-ion recombination coefficient with decreasing temperature (Fig. 4). The ion-ion recombination coefficient increased approximately by a factor of 5 (from 11.0×10^{-6} to 2.5×10^{-6} $cm^3 s^{-1}$) over the temperature range 218–293 K. This behavior seems not to be predicted by two of the three models and only partially by the third model, as shown in Fig. 6. Interestingly, all the models agree with each other and with the experimental results over a range of temperatures from 273 to 298 K, but there are big discrepancies in the absolute values as well as in the functional form of the temperature dependency at temperatures below 273 K. The model that seems to agree best with our data is the one by Brasseur and Chatel (1969), linked more directly to atmospheric data. The model by López-Yglesias and Flanagan (2013) that accounts accurately for all the possible physical processes does not agree with our data. Another option could be related to the evaporation of ions in the line. If the number of ions reaching the instrument was lower because of the losses for evaporation, the resulting recombination would be overestimated. The effect of the mixing fan and the chemical composition of the ions could vary with temperature, which would affect the recombination coefficient.

We observed a strong dependency of the recombination coefficient on relative humidity (RH). The ion-ion recombination coefficient decreases with decreasing RH from 9.4×10^{-6} to 2.0×10^{-6} $cm^3 s^{-1}$ as RH drops from 70 to 0 %, at a constant temperature of 298 K (Fig. 7). The decrease of the ion-ion recombination coefficient at increasing RH values could be related to an increase in size of the small ions: higher values of RH would form larger hydrated ions that would be less mobile, thus decreasing the recom-

ACPD
15, 3667–3702, 2015

bination rate. The change in ion mobility is plausible, as we know that aerosol particles with a diameter larger than 10 nm tend to be hygroscopic, changing their diameter according to the RH (Onasch et al., 1999; Keskinen et al., 2013). We also know, from quantum chemistry calculations, that ions form clusters with water and that the amount of water attached is dependent on RH (Kurten et al., 2007; Husar et al., 2012; Henschel et al., 2014; Olenius et al., 2014). This explanation matches the observed data qualitatively. In fact, according to quantum calculations shown in Kurten et al. (2007) for sulfuric acid ions at 20 % RH there are mostly 1 or 2 molecules of water in the cluster, whereas at 80 % RH there are 3 or 4. We get the equation below if we assume that the ions in the chamber: (1) are mainly sulfuric acid molecules, or behave the same way as sulfuric acid molecules, (2) are perfect spheres, and (3) that their mass is the sum of the masses of the molecules that compose the ions.

$$D_p = \sqrt[3]{\frac{6 \cdot (M_{H_2SO_4} + M_{H_2O} \cdot n_w)}{\pi \rho}} + 0.3\,\text{nm} \tag{8}$$

with

$$\rho = \rho(n_w) = \frac{M_{H_2SO_4} \cdot \rho_{H_2SO_4} + M_{H_2O} \cdot \rho_{H_2O} \cdot n_w}{M_{H_2SO_4} + n_w \cdot M_{H_2SO_4}} \tag{9}$$

Where D_p is the mobility diameter of the ions, $M_{H_2SO_4}$ and M_{H_2O} are the masses in Da of a sulfuric acid molecule and of a water molecule, respectively, n_w is the number of water molecules in a cluster and 0.3 nm is the difference between mobility diameter and mass diameter (Mäkelä et al., 1996; Ku and de la Mora, 2009). This calculation gives a D_p of 0.91–0.94 nm at 20 % RH and of 0.94–1.01 nm at 80 % RH. Unfortunately, the effect of RH on the ion diameter could not be observed directly, because this change in diameter is too small to be detected by the NAIS, given its low size resolution (Mirme and Mirme, 2013). However, the RH dependency of the recombination coefficient as a change in ion mobility is unclear, and cannot be predicted satisfactorily by any of the

ACPD
15, 3667–3702, 2015

models found in the literature; only the model by Gardner (1938) predicts an increase of the recombination coefficient for smaller ions, although it underestimates the absolute values.

4.2 Atmospheric implications

It is important to account for the ion-ion recombination when modelling ion concentrations. As described by Eq. (1), the term representing the ion-ion recombination is always present and becomes dominant for large ion production rates and when coagulation sinks are small, e.g. in the free troposphere (Volland, 1995).

The possibility of a strong dependency of the ion-ion recombination rate on temperature must be taken into account when interpreting and modelling data of ion concentration or ion production in environments or model domains with a large temperature variability. In fact, a change in temperature from −54 °C to 20 °C, a typical temperature change from the free troposphere down to the boundary layer, can cause a change in the recombination rate as high as one order of magnitude.

The RH seems to influence the rate of recombination as well, by decreasing the mobility of ions. In this study, the measurements at different RH were taken at constant temperature and, therefore, changes in RH reflect those in the absolute water vapor concentration. The lower the RH, the faster the ion loss via recombination was. This might be analogous to what happens at high altitudes, where water molecules are scarce.

It should be noted that, in the present study, the pressure was kept constant at +5 mbar above the atmospheric level during the experiments. In the atmosphere, however, a decrease in temperature with increasing altitude is associated with a decrease in pressure as well. In the CLOUD chamber it is not possible to lower the pressure below typical sea level values, as the chamber is not designed to withstand underpressure with respect to the outside pressure. So it was not possible to experimentally measure the variation of the ion-ion recombination rate at pressures lower than 900 hPa. It has been shown, however, that the ion-to-particle coefficients are consid-

ACPD
15, 3667–3702, 2015

erably different in ambient conditions at 20 km altitude than at ground level, with the recombination coefficient being an order of magnitude lower at 20 km altitude than at ground level López-Yglesias and Flanagan (2013). When moving from ground level to 20 km altitude, the decrease in the recombination coefficient due to decrease in pressure is only partly counterbalanced by the increase in the recombination coefficient due to decrease in temperature. Consequently, the pressure effect on the recombination coefficient needs to be taken into account when interpreting data measured at substantially different pressure than in this work, but investigating the pressure effect is beyond the scope of this study.

5 Conclusions

We carried out an experimental determination of the ion-ion recombination coefficient in the CLOUD chamber at CERN. The retrieved recombination coefficient at 20 °C and 40 % RH agrees with the literature values and with the models. We see no clear dependency of the ion-ion recombination rate coefficient for different ozone concentrations and only a weak variation at varying sulfur dioxide concentrations. Instead, we notice a strong dependency of the ion-ion recombination coefficient on temperature and relative humidity that has not been reported in previous studies. The ion-ion recombination coefficient varied between 9.7×10^{-6} and 2.3×10^{-6} $cm^3\,s^{-1}$ over the temperature range 220 to 293 K and between 9.3×10^{-6} and 1.5×10^{-6} $cm^3\,s^{-1}$ over the range of relative humidities from 0 to 70 %. The temperature dependency is not well described by any of the models found in the literature, only the model by Brasseur and Chatel (1969) seems to give results following the temperature dependence of our experimental data within 50 % uncertainty. The RH dependency of the ion-ion recombination coefficient is not well understood or described theoretically, but can be interpreted as an effect of ion hydration: when ions cluster with water molecules, their mobility decreases, and therefore they recombine at a lower rate. Only the model by Gardner (1938) shows

ACPD
15, 3667–3702, 2015

a functional dependency that supports this explanation, but it fails in reproducing the absolute values.

This was the first study to experimentally investigate the ion-ion recombination at atmospheric conditions. Our main finding was that the recombination coefficient depends strongly on temperature and relative humidity, quantities that have large variability in the troposphere. This work can be considered as a starting point for future studies in which pressure, chamber inhomogeneities and ion chemical composition could be taken into account.

Appendix A: Solution of the balance equation

The balance equation is expressed as following:

$$\frac{dn}{dt} = Q - \alpha n^2 - \beta n. \tag{A1}$$

The right hand term of Eq. (A1) is a second degree equation, therefore

$$\frac{dn}{dt} = -\alpha(n - n_1)(n - n_2), \tag{A2}$$

where:

$$n_1 = \frac{-\beta + \sqrt{\beta^2 + 4\alpha Q}}{2\alpha}$$

and

$$n_2 = \frac{-\beta - \sqrt{\beta^2 + 4\alpha Q}}{2\alpha}$$

are the solutions. Using the method of separation of variables (Eq. A2) becomes:

$$\frac{dn}{(n - n_1)(n - n_2)} = -\alpha dt \tag{A3}$$

ACPD
15, 3667–3702, 2015

Integrating, Eq. (A3) can be written as

$$\int_{n_0}^{n}\left(\frac{A}{n-n_1}+\frac{B}{n-n_2}\right)\mathrm{d}n=\int_{0}^{t}-\alpha\mathrm{d}t \tag{A4}$$

where n_0 is the ion concentration at $t = 0$ and $A(n-n_2)+B(n-n_1) = 1$. $A(n-n_2)+B(n-n_1) = 1$ can be written as $n(A+B)-(An_2+Bn_1) = 1$ and its solution is:

$$A=-B=\frac{1}{(n_1-n_2)}=\frac{\alpha}{\sqrt{\beta^2+4\alpha Q}}$$

As by solving Eq. (A4) we obtain:

$$A\ln\left(\frac{|n-n_1|}{|n_0-n_1|}\right)-A\ln\left(\frac{|n-n_2|}{|n_0-n_2|}\right)=-\alpha t$$

We can drop the absolute value because these values are always greater than zero:

$$A\ln\left(\frac{n-n_1}{n_0-n_1}\right)-A\ln\left(\frac{n-n_2}{n_0-n_2}\right)=-\alpha t$$

$$A\ln\left\{\frac{(n-n_1)(n_0-n_2)}{(n-n_2)(n_0-n_1)}\right\}=-\alpha t$$

$$\frac{(n-n_1)}{(n-n_2)}=\frac{(n_0-n_1)}{(n_0-n_2)}\exp\left(-\sqrt{\beta^2+4\alpha Q}t\right).$$

From this we can solve $n(t)$:

$$n(t)=\frac{(n_0-n_2)n_1-n_2(n_0-n_1)\exp(-t\sqrt{\beta^2+4\alpha Q})}{(n_0-n_2)-(n_0-n_1)\exp(-t\sqrt{\beta^2+4\alpha Q})} \tag{A5}$$

ACPD
15, 3667–3702, 2015

Acknowledgements. We would like to thank CERN for supporting CLOUD with important technical resources and for providing a particle beam from the CERN Proton Synchrotron. This research was funded by the European Commission 7th Framework Programme (Marie Curie Initial Training Network "CLOUD-ITN", grant 215072) , by the Academy of Finland via the Centre of Excellence Programme (project 1118615 and project 272041) and by the European Research Council (ERC) Advanced Grant Atmospheric nucleation: from molecular to global scale (ATMNUCLE) (grant 227463). Thanks to the German Federal Ministry of Education and Research (project no. 01LK0902A). J. Leppä would like to acknowledge the financial support from the Magnus Ehrnrooth Foundation, the Jane and Aatos Erkko Foundation and the Emil Aaltonen Foundation.

References

Adachi, M. and Kousaka, Y.: Unipolar and bipolar diffusion charging of ultrafine aerosol particles, J. Aerosol Sci., 16, 109–123, doi:10.1016/0021-8502(85)90079-5, 1985. 3670

Almeida, J., Schobesberger, S., Kurten, A. Ortega, I. K., Kupiainen-Maatta, O., Praplan, A. P., Adamov, A., Amorim, A., Bianchi, F., Breitenlechner, M., David, A., Dommen, J., Donahue, N. M., Downard, A., Dunne, E., Duplissy, J., Ehrhart, S., Flagan, R. C., Franchin, A., Guida, R., Hakala, J., Hansel, A., Heinritzi, M., Henschel, H., Jokinen, T., Junninen, H., Kajos, M., Kangasluoma, J., Keskinen, H., Kupc, A., Kurten, T., Kvashin, A. N., Laaksonen, A., Lehtipalo, K., Leiminger, M., Leppä, J., Loukonen, V., Makhmutov, V., Mathot, S., McGrath, M. J., Nieminen, T., Olenius, T., Onnela, A., Petäjä, T., Riccobono, F., Riipinen, I., Rissanen, M., Rondo, L., Ruuskanen, T., Santos, F. D., Sarnela, N., Schallhart, S., Schnitzhofer, R., Seinfeld, J. H., Simon, M., Sipilä, M., Stozhkov, Y., Stratmann, F., Tome, A., Trostl, J., Tsagkogeorgas, G., Vaattovaara, P., Viisanen, Y., Virtanen, A., Vrtala, A., Wagner, P. E., Weingartner, E., Wex, H., Williamson, C., Wimmer, D., Ye, P., Yli-Juuti, T., Carslaw, K. S., Kulmala, M., Curtius, J., Baltensperger, U., Worsnop, D. R., Vehkämäki, H., and Kirkby, J.: Molecular understanding of sulphuric acid-amine particle nucleation in the atmosphere, Nature, 502, 359–363, doi:dx.doi.org/10.1038/nature12663, 2013. 3679

Arnold, F.: Atmospheric ions and aerosol formation, Space. Sci. Rev., 137, 225–239, doi:10.1007/s11214-008-9390-8, 2008. 3670

ACPD
15, 3667–3702, 2015

Bates, D. R.: Recombination of small ions in the troposphere and lower stratosphere, Planet. Space Sci., 30, 1275–1282, doi:10.1016/0032-0633(82)90101-5, 1982. 3679
Bates, D. R. and Flannery, M. R.: Three-body ionic recombination at moderate and high gas densities, J. Phys. B-At. Mol. Opt., 2, 184–190, doi:10.1088/0022-3700/2/2/306, 1969. 3671
Brasseur, G. and Chatel, A.: Modeling of stratospheric ions: a first attempt, Presented at 9th Ann. Meeting of the European Geophys. Soc. Leeds, Great Britain, Aug. 1982, 1983. 3679, 3680, 3683
Carslaw, K. S., Harrison, R. G., and Kirkby, J.: Cosmic rays, clouds and climate, Science, 298, 1732–1737, 2002. 3669
Chalmers, J. A.: Atmospheric electricity, Clarendon Press, 1949. 3670
Chang, K.-N., Chen, Y.-K., Huang, S.-H., Chen, C.-W., Lai, C.-Y., and Chen, C.-C.: Penetration of charged particles through metallic tubes, J. Aerosol Sci., 48, 10–17, doi:10.1016/j.jaerosci.2012.01.006, 2012. 3680
Duplissy, J., Enghoff, M. B., Aplin, K. L., Arnold, F., Aufmhoff, H., Avngaard, M., Baltensperger, U., Bondo, T., Bingham, R., Carslaw, K., Curtius, J., David, A., Fastrup, B., Gagné, S., Hahn, F., Harrison, R. G., Kellett, B., Kirkby, J., Kulmala, M., Laakso, L., Laaksonen, A., Lillestol, E., Lockwood, M., Mäkelä, J., Makhmutov, V., Marsh, N. D., Nieminen, T., Onnela, A., Pedersen, E., Pedersen, J. O. P., Polny, J., Reichl, U., Seinfeld, J. H., Sipilä, M., Stozhkov, Y., Stratmann, F., Svensmark, H., Svensmark, J., Veenhof, R., Verheggen, B., Viisanen, Y., Wagner, P. E., Wehrle, G., Weingartner, E., Wex, H., Wilhelmsson, M., and Winkler, P. M.: Results from the CERN pilot CLOUD experiment, Atmos. Chem. Phys., 10, 1635–1647, doi:10.5194/acp-10-1635-2010, 2010. 3673, 3677
Gagné, S., Laakso, L., Petäjä, T., Kerminen, V.-M., Kulmala, M.: Analysis of one year of Ion-DMPS data from the SMEAR II station, Finland, Tellus B, 60, 318–319, 2008. 3669
Gardner, M. E.: The recombination of ions in pure oxygen as a function of pressure and temperature, Phys. Rev., 53, 75–83, doi:10.1103/PhysRev.53.75, 1938. 3678, 3682, 3683
Harrison, R. G. and Ambaum, M. H. P.: Enhancement of cloud formation by droplet charging, Proc. R. Soc., 464, 2561–2573, 2008. 3670
Harrison, R. G. and Carslaw, K. S.: Ion-aerosol-cloud processes in the lower atmosphere, Rev. Geophys., 41, 1012, doi:200310.1029/2002RG000114, 2003. 3670
Henschel, H., Navarro, J. C. A., Yli-Juuti, T., Kupiainen-Määttä, O., Olenius, T., Ortega, I. K., Clegg, S. L., Kurtén, T., Riipinen, I., and Vehkamäki, H.: Hydration of atmospherically rel-

ACPD
15, 3667–3702, 2015

evant molecular clusters: computational chemistry and classical thermodynamics, J. Phys. Chem. A, 118, 2599–2611, doi:10.1021/jp500712y, 2014. 3681

Hirsikko, A., Nieminen, T., Gagné, S., Lehtipalo, K., Manninen, H. E., Ehn, M., Hõrrak, U., Kerminen, V.-M., Laakso, L., McMurry, P. H., Mirme, A., Mirme, S., Petäjä, T., Tammet, H., Vakkari, V., Vana, M., and Kulmala, M.: Atmospheric ions and nucleation: a review of observations, Atmos. Chem. Phys., 11, 767–798, doi:10.5194/acp-11-767-2011, 2011. 3670

Hoppel, W. A. and Frich, G. M.: Ion-aerosol attachment coefficients and the steady-state charge distribution on aerosols in a bipolar ion environment, Aerosol Sci. Tech., 5, 1–21, doi:10.1080/02786828608959073, 1986. 3678

Hõrrak, U., Salm, J., and Tammet, H.: Statistical characterization of air ion mobility spectra at Tahkuse Observatory: classification of air ions, J. Geophys. Res., 105, 9291–9302, doi:200010.1029/1999JD901197, 2000. 3670

Husar, D. E., Temelso, B., Ashworth, A. L., and Shields, G. C.: Hydration of the bisulfate ion: atmospheric implications, J. Phys. Chem. A, 116, 5151–5163, doi:10.1021/jp300717j, 2012. 3681

Israël, H.: Atmospheric Electricity: Fundamentals, Conductivity, Ions, Israel Program for Scientific Translations, Jerusalem, 1970. 3669

Kazil, J. and Lovejoy, E. R.: Tropospheric ionization and aerosol production: a model study, J. Geophys. Res., 109, doi:200410.1029/2004JD004852, 2004. 3670, 3673

Kazil, J., Stier, P., Zhang, K., Quaas, J., Kinne, S., O'Donnell, D., Rast, S., Esch, M., Ferrachat, S., Lohmann, U., and Feichter, J.: Aerosol nucleation and its role for clouds and Earth's radiative forcing in the aerosol-climate model ECHAM5-HAM, Atmos. Chem. Phys., 10, 10733–10752, doi:10.5194/acp-10-10733-2010, 2010. 3670

Keskinen, H., Virtanen, A., Joutsensaari, J., Tsagkogeorgas, G., Duplissy, J., Schobesberger, S., Gysel, M., Riccobono, F., Slowik, J. G., Bianchi, F., Yli-Juuti, T., Lehtipalo, K., Rondo, L., Breitenlechner, M., Kupc, A., Almeida, J., Amorim, A., Dunne, E. M., Downard, A. J., Ehrhart, S., Franchin, A., Kajos, M.K. and Kirkby, J., Kürten, A., Nieminen, T., Makhmutov, V., Mathot, S., Miettinen, P., Onnela, A., Petäjä, T., Praplan, A., Santos, F. D., Schallhart, S., Sipilä, M., Stozhkov, Y., Tomé, A., Vaattovaara, P., Wimmer, D., Prevot, A., Dommen, J., Donahue, N. M., Flagan, R.C. and Weingartner, E., Viisanen, Y., Riipinen, I., Hansel, A., Curtius, J., Kulmala, M., Worsnop, D. R., Baltensperger, U., Wex, H., Stratmann, F., and Laaksonen, A.: Evolution of particle composition in CLOUD nucleation experiments, Atmos. Chem. Phys., 13, 5587–5600, doi:10.5194/acp-13-5587-2013, 2013. 3681

ACPD
15, 3667–3702, 2015

Kirkby, J., Curtius, J., Almeida, J., Dunne, E., Duplissy, J., Ehrhart, S., Franchin, A., Gagné, S., Ickes, L., Kürten, A., Kupc, A., Metzger, A., Riccobono, F., Rondo, L., Schobesberger, S., Tsagkogeorgas, G., Wimmer, D., Amorim, A., Bianchi, F., Breitenlechner, M., David, A., Dommen, J., Downard, A., Ehn, M., Flagan, R. C., Haider, S., Hansel, A., Hauser, D., Jud, W., Junninen, H., Kreissl, F., Kvashin, A., Laaksonen, A., Lehtipalo, K., Lima, J., Lovejoy, Edward R., Makhmutov, V., Mathot, S., Mikkilä, J., Minginette, P., Mogo, S., Nieminen, T., Onnela, A., Pereira, P., Petäjä, T., Schnitzhofer, R., Seinfeld, J. H., Sipilä, M., Stozhkov, Y., Stratmann, F., Tomé, A., Vanhanen, J., Viisanen, Y., Vrtala, A., Wagner, P. E., Walther, H., Weingartner, E., Wex, H., Winkler, P. M., Carslaw, K. S., Worsnop, D. R., Baltensperger, U., and Kulmala, M.: Role of sulphuric acid, ammonia and galactic cosmic rays in atmospheric aerosol nucleation, Nature, 476, 429–433, doi:10.1038/nature10343, 2011. 3669, 3672

Kontkanen, J., Lehtinen, K. E. J., Nieminen, T., Manninen, H. E., Lehtipalo, K., Kerminen, V.-M., and Kulmala, M.: Estimating the contribution of ion-ion recombination to sub-2 mm cluster concentrations from atmospheric measurements, Atmos. Chem. Phys., 13, 11391–11401, doi:10.5194/acp-13-11391-2013, 2013. 3670

Ku, B. K. and de la Mora, J. F.: Relation between electrical mobility, mass, and size for nanodrops 1–6.5 nm in diameter in air, Aerosol Sci. Tech., 43, 241–249, doi:10.1080/02786820802590510, 2009. 3681

Kulmala, M., Maso, M. D., Mäkelä, J. M., Pirjola, L., Väkevä, M., Aalto, P., Miikkulainen, P., Hämeri, K., and O'Dowd, C. D.: On the formation, growth and composition of nucleation mode particles, Tellus B, 53, 479–490, doi:10.1034/j.1600-0889.2001.530411.x, 2001. 3676

Kulmala, M., Riipinen, I., Sipilä, M., Manninen, H. E, Petäjä, T., Junninen, H., Dal Maso, M., Mordas, G., Mirme, A., Vana, M., Hirsikko, A., Laakso, L., Harrison, R. M., Hanson, I., Leung, C., Lehtinen, K. E. J., and Kerminen, V.-M.: Toward direct measurement of atmospheric nucleation, Science, 318, 89–92, doi:10.1126/science.1144124, 2007. 3675

Kulmala, M., Kontkanen, J., Junninen, H., Lehtipalo, K., Manninen, H. E., Nieminen, T., Petaja, T., Sipila, M., Schobesberger, S., Rantala, P., Franchin, A., Jokinen, T., Jarvinen, E., Aijala, M., Kangasluoma, J., Hakala, J., Aalto, P. P., Paasonen, P., Mikkila, J., Vanhanen, J., Aalto, J., Hakola, H., Makkonen, U., Ruuskanen, T., Mauldin, R. L., Duplissy, J., Vehkämäki, H., Back, J., Kortelainen, A., Riipinen, I., Kurten, T., Johnston, M. V., Smith, J. N., Ehn, M., Mentel, T. F., Lehtinen, K. E. J., Laaksonen, A., Kerminen, V.-M., and Worsnop, D. R.: Direct observations of atmospheric aerosol nucleation, Science, 339, 943–946, doi:10.1126/science.1227385, 2013. 3670

ACPD
15, 3667–3702, 2015

Kupc, A., Amorim, A., Curtius, J., Danielczok, A., Duplissy, J., Ehrhart, S., Walther, H., Ickes, L., Kirkby, J., Kürten, A., Lima, J. M., Mathot, S., Minginette, P., Onnela, A., Rondo, L., and Wagner, P. E.: A fibre-optic UV system for H_2SO_4 production in aerosol chambers causing minimal thermal effects, J. Aerosol Sci., 42, 532–543, 2011. 3673

Kurtén, T., Noppel, M., Vehkamäki, H., Salonen, M., and Kulmala, M.: Quantum chemical studies of hydrate formation of H_2SO_4 and HSO_4^-–, Bor. Env. Res., 12, 431–453, 2007. 3681

Laakso, L., Petäjä, T., Lehtinen, K. E. J., Kulmala, M., Paatero, J., Hõrrak, U., Tammet, H., and Joutsensaari, J.: Ion production rate in a boreal forest based on ion, particle and radiation measurements, Atmos. Chem. Phys., 4, 1933–1943, doi:10.5194/acp-4-1933-2004, 2004. 3670, 3679

Leppä, J., Anttila, T., Kerminen, V.-M., Kulmala, M., and Lehtinen, K. E. J.: Atmospheric new particle formation: real and apparent growth of neutral and charged particles, Atmos. Chem. Phys., 11, 4939–4955, doi:10.5194/acp-11-4939-2011, 2011. 3676

Loeb, L. B.: Basic Processes of Gaseous Electronics, University of California Press, 1955. 3678

López-Yglesias, X. and Flanagan, R. C.: Ion-aerosol flux coefficients and the steady-state charge distribution of aerosols in a bipolar ion environment, Aerosol Sci. Tech., 47, 688–704, doi:10.1080/02786826.2013.783684, 2013. 3678, 3680, 3683

Mäkelä, J. M., Riihelä, M., Ukkonen, A., Jokinen, V., and Keskinen, J.: Comparison of mobility equivalent diameter with Kelvin–Thomson diameter using ion mobility data, J. Chem. Phys., 105, 1562–1571, doi:10.1063/1.472017, 1996. 3670, 3681

Manninen, H. E., Petäjä, T., Asmi, E., Riipinen, I., Nieminen, T., Mikkilä, J., Hõrrak, U., Mirme, A., Mirme, S., Laakso, L., Kerminen, V.-M., and Kulmala, M.: Long-term field measurements of charged and neutral clusters using Neutral cluster and Air Ion Spectrometer (NAIS), Boreal Environ. Res., 14, 591–605, 2009. 3675

Manninen, H. E., Nieminen, T., Asmi, E., Gagné, S., Häkkinen, S., Lehtipalo, K., Aalto, P., Vana, M., Mirme, A., Mirme, S., Hõrrak, U., Plass-Dülmer, C., Stange, G., Kiss, G., Hoffer, A., Törő, N., Moerman, M., Henzing, B., de Leeuw, G., Brinkenberg, M., Kouvarakis, G. N., Bougiatioti, A., Mihalopoulos, N., O'Dowd, C., Ceburnis, D., Arneth, A., Svenningsson, B., Swietlicki, E., Tarozzi, L., Decesari, S., Facchini, M. C., Birmili, W., Sonntag, A., Wiedensohler, A., Boulon, J., Sellegri, K., Laj, P., Gysel, M., Bukowiecki, N., Weingartner, E., Wehrle, G., Laaksonen, A., Hamed, A., Joutsensaari, J., Petäjä, T., Kerminen, V.-M., and Kulmala, M.: EUCAARI ion spectrometer measurements at 12 European sites – analysis

ACPD
15, 3667–3702, 2015

of new particle formation events, Atmos. Chem. Phys., 10, 7907–7927, doi:10.5194/acp-10-7907-2010, 2010. 3670
Manninen, H. E., Franchin, A., Schobesberger, S., Hirsikko, A., Hakala, J., Skromulis, A., Kangasluoma, J., Ehn, M., Junninen, H., Mirme, A., Mirme, S., Sipilä, M., Petäjä, T., Worsnop, D. R., and Kulmala, M.: Characterisation of corona-generated ions used in a Neutral cluster and Air Ion Spectrometer (NAIS), Atmos. Meas. Tech., 4, 2767–2776, doi:10.5194/amt-4-2767-2011, 2011. 3670
Mayya, Y. S. and Sapra, B. K.: Image forces on a collection of charged particles near conducting surfaces, J. Aerosol Sci., 5, 817–828, doi:10.1016/S0021-8502(02)00038-1, 2002. 3679
McGowan, S.: Ion-ion recombination in laboratory air, Phys. Med. Biol., 10, 25–40, doi:10.1088/0031-9155/10/1/303, 1965. 3671
McMurry, P. H. and Rader, D. J.: Aerosol wall losses in electrically charged chambers, Aerosol Sci. Tech. 4, 249–268, doi:10.1080/02786828508959054, 1985. 3672, 3679
Mirme, S. and Mirme, A.: The mathematical principles and design of the NAIS – a spectrometer for the measurement of cluster ion and nanometer aerosol size distributions, Atmos. Meas. Tech., 6, 1061–1071, doi:10.5194/amt-6-1061-2013, 2013. 3675, 3681
Mizin, S. V., Makhmutov, V. S., Maksumov, O. S., and Kvashnin, A. N.: Application of multithreading programming to physical experiment, B. Lebedev Phys. Inst., 38, 34–40, doi:10.3103/S1068335611020023, 2011. 3674
Natanson, G. L.: On the theory of the charging of a microscopic aerosol particles as a result of capture of gas ions, Zh. Tekh. Fiz. (Transl.), 30, 573–588, 1960. 3671
Ogawa, T.: Fair-weather electricity, J. Geophys. Res.-Atmos., 90, 5951–5960, doi:10.1029/JD090iD04p05951, 1985. 3670
Olenius, T., Kurtén, T., Kupiainen-Määttä, O., Henschel, H., Ortega, I. K., and Vehkamäki, H.: Effect of hydration and base contaminants on sulfuric acid diffusion measurement: a computational study, Aerosol Sci. Tech., 48, 593–603, doi:10.1080/02786826.2014.903556, 2014. 3681
Onasch, T. B., Siefert, R. L., Brooks, S. D., Prenni, A. J., Murray, B., Wilson, M. A., and Tolbert, M. A.: Infrared spectroscopic study of the deliquescence and efflorescence of ammonium sulfate aerosol as a function of temperature, J. Geophys. Res.-Atmos., 104, 21317–21326, doi:10.1029/1999JD900384, 1999. 3681
Schnitzhofer, R., Metzger, A., Breitenlechner, M., Jud, W., Heinritzi, M., De Menezes, L.-P., Duplissy, J., Guida, R., Haider, S., Kirkby, J., Mathot, S., Minginette, P., Onnela, A., Walther, H.,

ACPD
15, 3667–3702, 2015

Wasem, A., Hansel, A., and the CLOUD Team: Characterisation of organic contaminants in the CLOUD chamber at CERN, Atmos. Meas. Tech., 7, 2159–2168, doi:10.5194/amt-7-2159-2014, 2014. 3673
Smirnov, I. B.: Modeling of ionization produced by fast charged particles in gases, Nucl. Instrum. Meth. A, 554, 474–493, doi:10.1016/j.nima.2005.08.064, 2005. 3677
Smith, D. and Adams, N. G.: Ionic recombination in the stratosphere, Geophys. Res. Lett., 9, 1085–1087, doi:10.1029/GL009i009p01085, 1982. 3679
Smith, D. and Spanel, P.: Ions in the terrestrial atmosphere and in interstellar clouds, Mass Spectrom. Rev., 14, 255–278, doi:10.1002/mas.1280140403, 1995. 3670, 3671
Tammet, H., Hõrrak, U., Laakso, L., and Kulmala, M.: Factors of air ion balance in a coniferous forest according to measurements in Hyytiälä, Finland, Atmos. Chem. Phys., 6, 3377–3390, doi:10.5194/acp-6-3377-2006, 2006. 3671
Thomson, J. J. and Thomson, G. P.: Conduction of Electricity Through Gases: Volume 1, Ionisation by Heat and Light, Cambridge University Press, 2013. 3678
Tinsley, B. A.: Influence of solar wind on the global electric circuit, and inferred effects on cloud microphysics, temperature, temperature, and dynamics in the troposphere, Space Sci. Rev., 94, 231–258, 2000. 3670
Usoskin, I. G. and Kovaltsov, G. A.: Cosmic rays and climate of the Earth: possible connection, C. R. Geosci., 340, 441–450, 2008. 3669
Vauge, C.: On the concept of “image-force”, J. Aerosol Sci., 33, 829–832, doi:10.1016/S0021-8502(02)00037-X, 2002. 3679
Voigtländer, J., Duplissy, J., Rondo, L., Kürten, A., and Stratmann, F.: Numerical simulations of mixing conditions and aerosol dynamics in the CERN CLOUD chamber, Atmos. Chem. Phys., 12, 2205–2214, doi:10.5194/acp-12-2205-2012, 2012. 3674
Volland, H.: Handbook of Atmospheric Electrodynamics, CRC Press, 1995. 3671, 3682
Williams, A. G., Zahorowski, W., Chambers, S., Griffiths, A., Hacker, J. M., Element, A., and Werczynski, S.: The vertical distribution of radon in clear and cloudy daytime terrestrial boundary layers, J. Atmos. Sci., 68, 155–174, doi:10.1175/2010JAS3576.1, 2011. 3670
Yu, F., Luo, G., Bates, T. S., Anderson, B., Clarke, A., Kapustin, V., Yantosca, R. M., Wang, Y., and Wu, S.: Spatial distributions of particle number concentrations in the global atmosphere: simulations, observations, and implications for nucleation mechanisms, J. Geophys. Res., 115, D17205, doi:10.1029/2009JD013473, 2010. 3670

ACPD
15, 3667–3702, 2015

Zhang, K., Feichter, J., Kazil, J., Wan, H., Zhuo, W., Griffiths, A. D., Sartorius, H., Zahorowski, W., Ramonet, M., Schmidt, M., Yver, C., Neubert, R. E. M., and Brunke, E.-G.: Radon activity in the lower troposphere and its impact on ionization rate: a global estimate using different radon emissions, Atmos. Chem. Phys., 11, 7817–7838, doi:10.5194/acp-11-7817-2011, 2011. 3670, 3673

ACPD
15, 3667–3702, 2015

Table 1. Values of the recombination coefficient and its uncertainty at different temperatures. The uncertainty reported is calculated with error propagation and includes the uncertainty in the fit.

T (°C)	$\alpha \times 10^{-6}$ ($cm^3 s^{-1}$)	$\sigma_\alpha \times 10^{-6}$ ($cm^3 s^{-1}$)
20	2.3	0.7
5	1.6	0.6
−25	7.6	1.0
−55	9.7	1.2

ACPD
15, 3667–3702, 2015

Table 2. Values of the recombination coefficient and its uncertainty at different relative humidities. The uncertainty reported is calculated with error propagation and includes the uncertainty in the fit.

RH (%)	$\alpha \times 10^{-6}$ ($cm^3 s^{-1}$)	$\sigma_\alpha \times 10^{-6}$ ($cm^3 s^{-1}$)
70	2.0	0.7
40	2.3	0.7
7	8.1	2.8
0	9.9	3.0

ACPD
15, 3667–3702, 2015

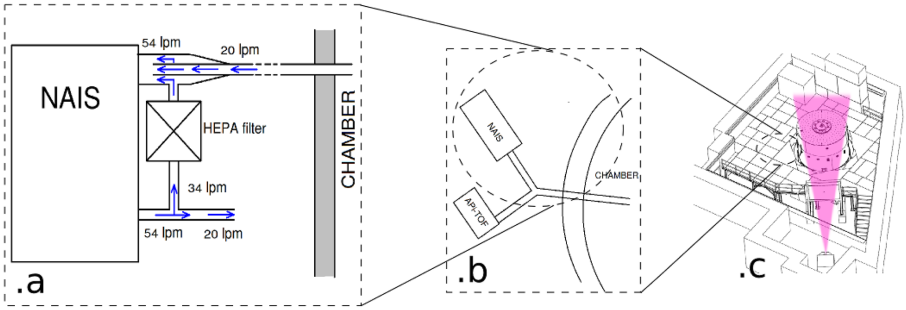

Figure 1. (a) Neutral cluster and Air Ion Spectrometer (NAIS) and its dilution system used during the CLOUD experiments. The sample air flow is withdrawn from the chamber at a flow rate that varies between 20 and 30 L min^{-1}. The sample air from the chamber is diluted with a portion of the exhaust air of the instrument, which is filtered with a High Efficiency Particulate Air (HEPA) filter and mixed with the sample air. **(b)** Configuration of the NAIS during the CLOUD experiments. **(c)** Sketch of the chamber and the beam. The dashed circle represents the area where the NAIS was located, outside of the beam trajectory. The beam is deliberately defocused to maximize the volume in the chamber where ionization takes place.

ACPD
15, 3667–3702, 2015

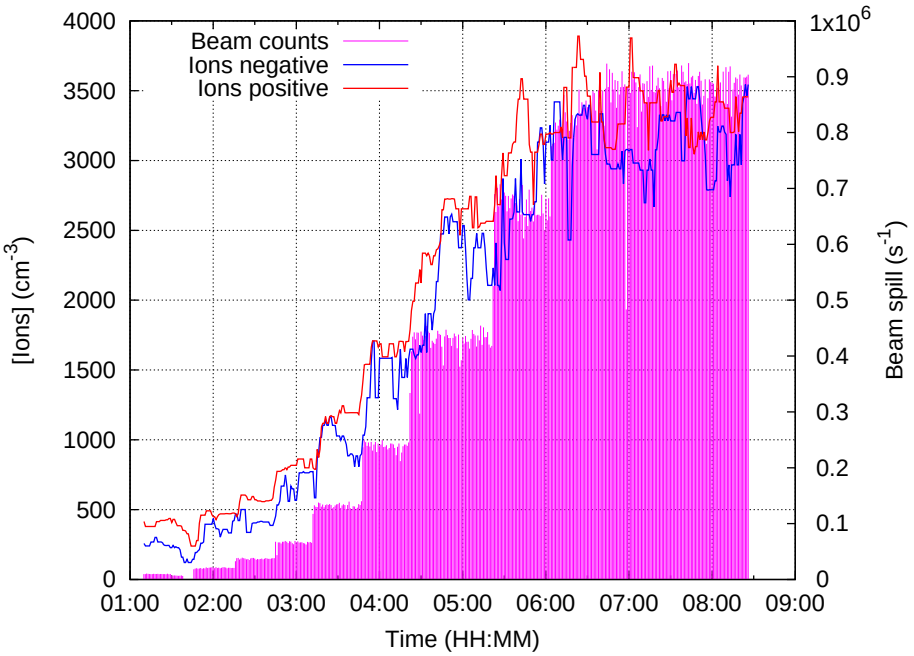

Figure 2. In a typical experiment, the beam intensity is varied, changing the flux of pions crossing the chamber. The beam intensity is directly proportional to the Ion Production Rate (IPR) and is kept constant for a period of approximately 30 min at each step, to make sure that the ion concentration reaches the steady state. The mean ion concentration is related to the mean IPR at steady state via the balance equation (Eq. 1). Blue and red colors correspond to negative and positive ions, respectively. The beam intensity is shown in magenta.

ACPD
15, 3667–3702, 2015

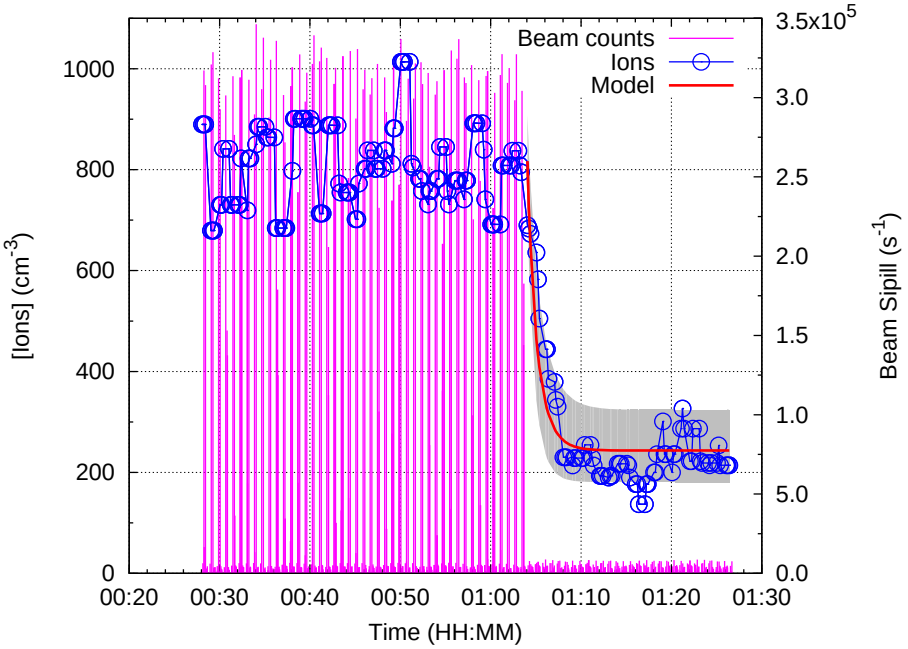

Figure 3. The ion concentration (blue line and circles), the solution to Eq. (1) (red line) and the beam counts (magenta line). When solving Eq. (1), the recombination coefficient and linear loss term, retrieved independently by fitting the steady state balance equation at the same conditions (T = 293 K, RH = 0 %), were 9.3×10^{-6} cm^3 s^{-1} and 8.3×10^{-3} s^{-1}, respectively, and the ion production rate was 8.3 cm^{-3} s^{-1}. The initial concentration of small ions, n_0 (t = 01:03), was 810 cm^{-3} (average over time range from 00:24 to 01:03). The grey shaded area is the model uncertainty assuming uncertainty of ±30 % on n_0, α and β.

ACPD
15, 3667–3702, 2015

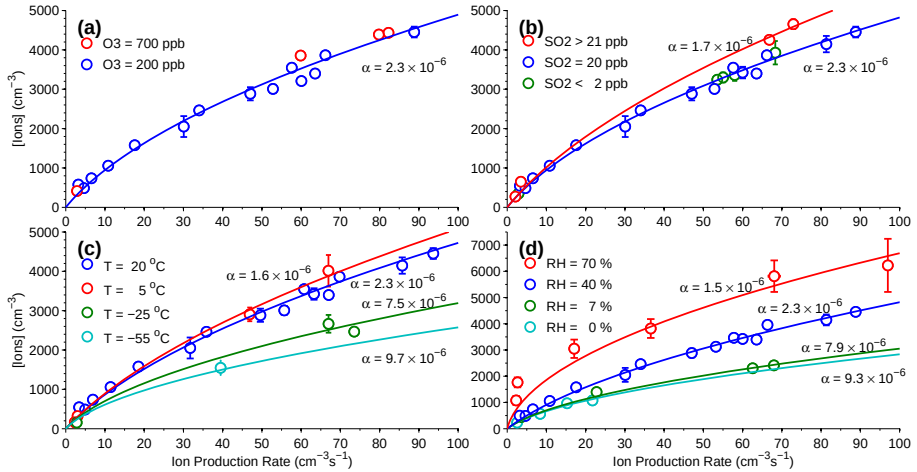

Figure 4. Ion concentration as a function of ion production rate at **(a)** two different ozone concentrations (at 200 ppb and at 700 ppb); the other variables were kept constant ($T = 20\,^{\circ}C$, RH = 40 % and $[SO_2] = 20$ ppb); **(b)** different SO_2 concentrations between 2 and 30 ppb, temperature, RH and ozone concentration were kept constant ($T = 20\,^{\circ}C$, RH = 40 % and $[SO_2] = 20$ ppb); **(c)** different temperatures (20, 5, −25 and −55 °C); and **(d)** different relative humidities (0, 7, 40 and 70 %) at a constant temperature of 20 °C.

ACPD
15, 3667–3702, 2015

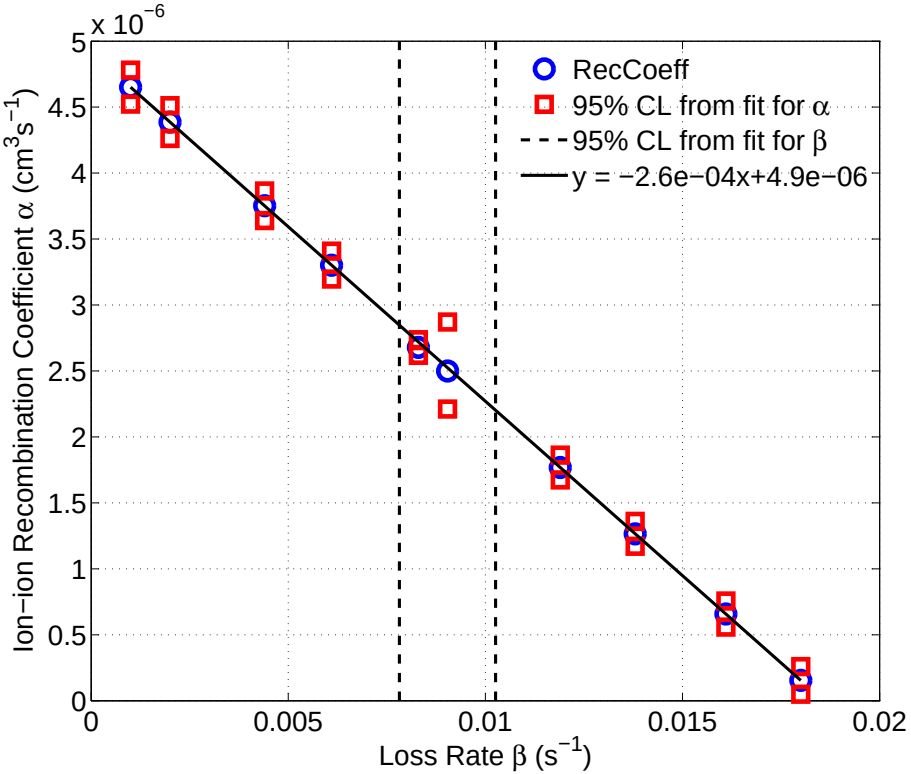

Figure 5. Variability of the retrieved recombination rate as a function of loss rate. The dataset used here includes experiments performed at T = 20 °C and RH = 40 %. The point at the center presents the larger confidence level interval as the loss term was kept as a free parameter. The other points were obtained by forcing the loss term β to values varying from 1×10^{-3} to 0.18 s^{-1}.

ACPD
15, 3667–3702, 2015

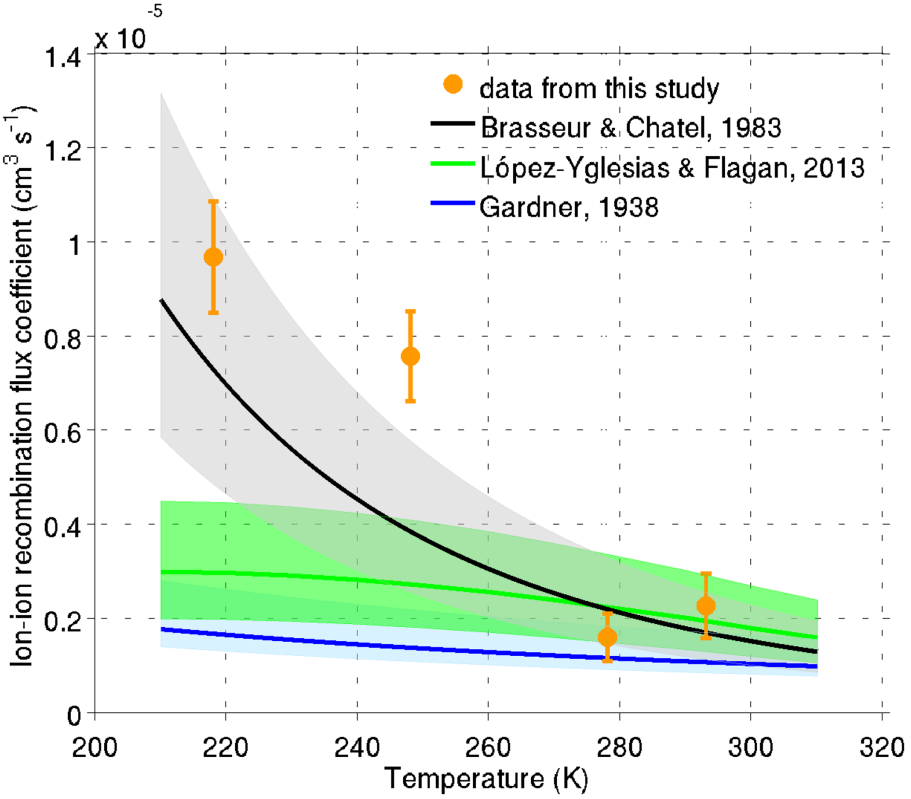

Figure 6. A comparison between the ion-ion recombination coefficient, measured at different temperatures (points with error bars) and the recombination coefficient modelled using different models. The shaded area represents 50 % uncertainty.

ACPD
15, 3667–3702, 2015

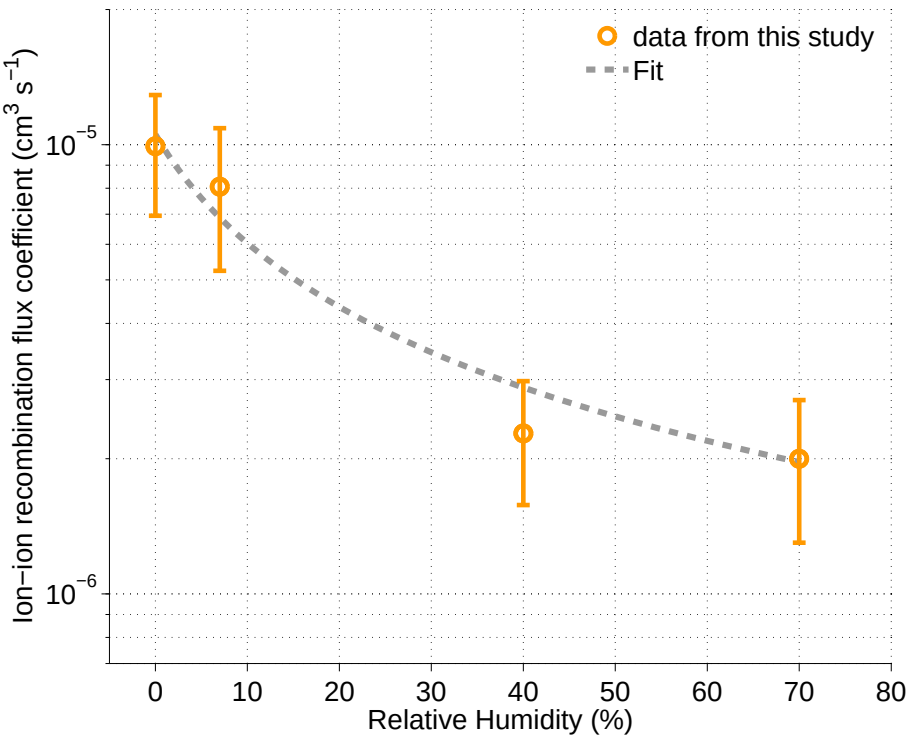

Figure 7. The ion-ion recombination coefficient measured at different relative humidities, at a constant temperature of 20 °C. The dots are measured points, the dashed line is an exponential fit to guide the eye.

ACPD
15, 3667–3702, 2015